JGR Oceans

RESEARCH ARTICLE
10.1029/2018JC014628

Disentangling the Mesoscale Ocean-Atmosphere Interactions

L. Renault[1,2], S. Masson[3], V. Oerder[4,5], S. Jullien[6], and F. Colas[3]

[1]LEGOS, University of Toulouse, IRD, CNRS, CNES, UPS, Toulouse, France, [2]Atmospheric and Oceanic Sciences, University of California, Los Angeles, CA, USA, [3]LOCEAN-IPSL, Sorbonne Universités (UPMC)/IRD/CNRS/MNHN, UMR7159, Paris, France, [4]Escuela de Ciencias del Mar and Instituto Milenio de Oceanografia, Pontificia Universidad Catolica de Valparaiso, Valparaiso, Chile, [5]Millennium Institute of Oceanography (IMO), University of Concepcion, Concepcion, Chile, [6]Ifremer, Universite Brest, CNRS, IRD, Laboratoire d'Oceanographie Physique et Spatiale, IUEM, Brest, France

Key Points:
- The mesoscale ocean current feedback effect (CFB) on surface wind and stress can be unraveled from that due to the thermal feedback (TFB)
- The TFB effect on surface wind and stress curl is contaminated by the CFB effect
- Surface stress is an appropriate variable to assess mesoscale air-sea coupling from scatterometer data

Correspondence to:
L. Renault,
lionel.renault@ird.fr

Citation:
Renault, L., Masson, S., Oerder, V., Jullien, S., & Colas, F. (2019). Disentangling the mesoscale ocean-atmosphere interactions. *Journal of Geophysical Research: Oceans*, *124*, 2164–2178. https://doi.org/10.1029/2018JC014628

Received 8 OCT 2018
Accepted 10 MAR 2019
Accepted article online 14 MAR 2019
Published online 28 MAR 2019

Abstract In the past decades, the use of scatterometer data allowed to demonstrate the global ubiquity of the ocean mesoscale thermal feedback (TFB) and current feedback (CFB) effects on surface winds and stress. Understanding these air-sea interactions is of uttermost importance as the induced atmospheric anomalies partly control the ocean circulation and thus can influence the Earth climate. Whether the TFB and CFB effects can be disentangled, and whether satellite scatterometers can properly reveal them, remain rather unclear. Here, using satellite observations and ocean-atmosphere coupled mesoscale simulations over 45°S to 45°N, we show that the CFB effect can be properly characterized and unraveled from that due to the TFB. We demonstrate that the TFB can be unambiguously characterized by its effect on the stress (and wind) divergence and magnitude. However, its effect on the wind and stress curl is contaminated by the CFB and thus cannot be estimated from scatterometer data. Finally, because scatterometers provide equivalent neutral stability winds relative to the oceanic currents, they cannot characterize adequately the CFB wind response and overestimate the TFB wind response by ≈25%. Surface stress appears to be the more appropriate variable to consider from scatterometer data.

1. Introduction

In the past decades, air-sea interactions at the oceanic mesoscale (i.e., scales of tens to hundreds of kilometers and tens to hundreds of days, e.g., Chelton et al., 2007; McWilliams, 2008; Stammer, 1997; Wunsch & Stammer, 1995) have received a growing interest from the scientific community (Chelton & Xie, 2010) and have been shown to have a large influence on both wind and surface stress (Chelton et al., 2001, 2007; Gaube et al., 2015; O'Neill et al., 2012; Perlin et al., 2014; Renault, Molemaker, Mcwilliams, et al., 2016). In the literature, two main interactions have been assessed: the influence of the sea surface temperature (SST) on the atmosphere, that is, the thermal feedback (TFB) and the influence of the surface oceanic currents on the surface stress and wind, that is, the current feedback (CFB).

The TFB has a "top-down" effect: it modifies the atmospheric boundary layer (ABL) turbulence and the wind, which consequently alter the surface stress. In that case, the surface stress-induced anomalies are directly related and positively correlated to the wind-induced anomalies (Chelton et al., 2004). Small et al. (2008) provide a review of the different processes involved. The TFB has a linear effect on the stress and the wind curl, divergence, and magnitude (Chelton & Xie, 2010; Chelton et al., 2004; O'Neill et al., 2003; Small et al., 2009). This has been quantified by coupling coefficients (Chelton et al., 2007, 2011; Desbiolles et al., 2016; Oerder et al., 2016; O'Neill et al., 2012; Perlin et al., 2014; Wang & Castelao, 2016) defined between (see section 2 and Table 1 for a complete description): wind/stress curl and cross-wind/stress SST gradient (s_{Cu}/s_{Cstr}); wind/stress divergence and down-wind/stress SST gradient (s_{Du}/s_{Dstr}); wind/stress speed anomalies and SST anomalies (S_u/S_{str}). On the oceanic side, Hogg et al. (2009), using a high-resolution quasigeostrophic ocean model, suggest that the mesoscale TFB could slow down the large-scale currents. More recently, Ma et al. (2016) and Seo (2017) suggested that the TFB generates wind velocity and turbulent heat fluxes anomalies that could impact the western boundary currents (WBCs).

The surface oceanic currents are generally much weaker than the winds, but their interactions with the surface wind and stress (the CFB) influence both the atmosphere and the ocean (e.g., Bye, 1985; Rooth & Xie,

Table 1
Coupling Coefficients

Coefficient	Description
s_r	Surface current vorticity and surface stress curl
s_w	Surface current vorticity and wind curl
s_{Cstr}	Cross-wind SST and surface stress curl
s_{Cu}	Cross-wind SST and 10-m wind curl
s_{Dstr}	Down-wind SST and surface stress divergence
s_{Du}	Down-wind SST and 10-m wind divergence
s_{str}	SST and surface stress magnitude
s_u	SST and 10-m wind magnitude

1992; Dewar & Flierl, 1987; Duhaut & Straub, 2006; Eden & Dietze, 2009; McClean et al., 2011; Hutchinson et al., 2010; Anderson et al., 2011; Renault, Molemaker, Mcwilliams, et al. 2016; Renault, McWilliams, Masson, et al., 2017); Oerder et al., 2018). Contrarily to the TFB, the CFB modifies directly the surface stress (Bye, 1985; Chelton et al., 2001) and has a "bottom-up" effect on the wind: a positive current anomaly creates a negative stress anomaly, which in turn causes a positive wind anomaly (Renault, Molemaker, Mcwilliams, et al., 2016; Takatama & Schneider, 2017). Therefore, wind and stress anomalies induced by the CFB are anti-correlated. Although the CFB modifies directly the surface stress, it does not have statistically a systematic effect on the stress (wind) magnitude as a current anomaly can induce a positive or a negative stress (wind) anomaly depending on the wind direction. At the mesoscale, the ocean currents are very nearly geostrophic and mainly nondivergent, so that the mesoscale CFB mainly affects the stress (wind) curl but not its divergence (Chelton et al., 2004; Oerder et al., 2018; O'Neill et al., 2003; Renault, Molemaker, Mcwilliams, et al., 2016; Renault, McWilliams, Masson, et al., 2017) demonstrate that the CFB causes surface stress/wind curl anomalies that are both linearly related to the current vorticity. They define two additional coupling coefficients: one between surface current vorticity and stress curl (s_r); and one between surface current vorticity and wind curl (s_w). The CFB slows down the mean oceanic currents (e.g., Pacanowski, 1987; Luo et al., 2005) and induces a dampening of the eddy mesoscale activity by ≈30% by acting as an "eddy killer," that is, by causing a sink of energy from the eddies to the atmosphere (e.g., Anderson et al., 2011; Bye, 1985; Dewar & Flierl, 1987; Duhaut & Straub, 2006; Eden & Dietze, 2009; Hutchinson et al., 2010; McClean et al., 2011; Oerder et al., 2018; Renault, Molemaker, Mcwilliams, et al., 2016, Renault, McWilliams, Masson, et al., 2017; Rooth & Xie, 1992; Xu & Scott, 2008). It appears crucial to represent the CFB in numerical oceanic models as it partly controls the WBCs dynamics (Renault et al., 2019; Renault, Molemaker, Gula, et al., 2016, Renault, McWilliams, Penven, et al., 2017). Characterizing and modeling the mesoscale air-sea interactions and their consequences on the ocean dynamics and biogeochemistry is therefore of uttermost importance.

Scatterometers such as QuikSCAT have been largely used to characterize the wind/stress responses to the mesoscale TFB and CFB. Scatterometers represent a unique measurement technique that allowed the scientific community to improve its understanding of the air-sea interactions. In particular they have been used to demonstrate the global ubiquity and the seasonality of both TFB and CFB effects on surface winds at oceanic mesoscale (see, e.g., Kelly et al., 2001; Cornillon & Park, 2001; Chelton et al. (2001, 2004); Chelton and Xie 2010; O'Neill et al., 2010, 2012; Renault, McWilliams, Masson, et al., 2017). They have also motivated models development and analysis, like the study presented here. As detailed in section 2, within a scatterometer framework, an important point to clarify is the definition of the 10-m wind. Hereinafter, the 10-m wind U_a is defined as the absolute wind at the first vertical level of the atmospheric model (which has been defined at ≈10 m), whereas the relative wind U_r is defined as the difference between U_a and the surface oceanic currents. Satellite scatterometers (such as QuikSCAT) provide a 10-m wind that does not correspond to U_a. It is reported as the so-called equivalent neutral stability wind (U_{ENW}, Ross et al., 1985, see section 2). Based on in situ data analysis, the ENW has been shown to overestimate U_a and its mesoscale response to the TFB from 10% to 30% (Liu & Tang, 1996; Liu et al., 2007; O'Neill, 2012; O'Neill et al., 2010). Moreover, as suggested by, for example, Chelton et al. (2001); Kelly et al. (2001), Cornillon and Park (2001), and Plagge et al. (2012), scatterometers winds represent the ENW (U_{ENWr}) relative to the surface currents rather than the absolute ENW. Scatterometers may therefore induce errors in the characterization of the TFB and CFB effects on the wind.

Both TFB and CFB affect the stress and the wind but because the mesoscale currents are very nearly geostrophic (thus, very often proportional and perpendicular to the SST gradients), the stress mesoscale anomalies induced by the CFB can also be proportional and perpendicular to the SST gradients (Perlin et al., 2014). Chelton et al. (2001) suggest that the TFB effect on wind stress curl observed by scatterometers could be contaminated by the CFB effect. So far, it is still unclear how to unravel the TFB effect from that due to the CFB and thus whether the defined coupling coefficients allow to properly separate the mesoscale TFB and CFB effects on wind and surface stress. Without consistent measurements of surface ocean velocity, it is not possible to separate the effects of TFB and CFB on the curl fields. So far, only coupled models can be used to separate the CFB effect from the TFB effects. Using a numerical model off California, Renault, Molemaker, Mcwilliams, et al. (2016) recently showed that the coupling coefficients s_τ and s_w allow to distinguish the CFB from the TFB effect on the surface stress and on the wind. However, this has not been yet demonstrated globally.

In this study, a set of three realistic mesoscale-resolving ocean and atmosphere-coupled simulations are carried out over the region 45°S to 45°N (Samson et al., 2017) for a period of 5 years. The simulations differ by the coupling effects they are resolving, including or not the mesoscale TFB and the CFB (see section 2). Based on these simulations and available satellite data, the aim of this study is twofold. First, it strives to assess to what extent the various coupling coefficients allow disentangling the TFB from the CFB. Second, it aims to determine whether scatterometers can adequately monitor the wind and stress responses to mesoscale air-sea coupling.

2. Data, Models, and Methods Description

2.1. Data

2.1.1. Surface Stress and Wind From QuikSCAT

The surface stress and ENW are obtained from the QuikSCAT gridded product from Ifremer (Bentamy et al., 2013) for the period 2000–2008. It has a spatial resolution of 0.25°.

2.1.2. AVISO Altimetry

The daily absolute dynamic topography fields are obtained from the AVISO product (Ducet et al., 2000) for the period 2000–2008. The sea level anomaly data are based on a square grid of 0.25°. The daily absolute dynamic topography maps are then produced by adding the mean dynamic topographic data to the sea level anomaly (Rio et al., 2014).

2.1.3. SST

The daily SST fields used here have a spatial resolution of 0.25° and are obtained from the OI SST analysis version 2 over the time period 2000–2008. A full description of the complete analysis procedure can be found in Reynolds et al. (2007).

2.2. Model Description

The numerical models and configurations are the same as the ones employed in Samson et al. (2017), and the following models' descriptions are derived from there. The oceanic simulations were performed with the Nucleus for European Modelling of the Ocean (NEMO) v3.4. A complete description of this model can be found in Madec and The NEMO team (2015). The atmospheric component is the Weather Research and Forecasting (WRF) version 3.3.1, which solves compressible, nonhydrostatic Euler equations with the Advanced Research WRF (ARW) dynamical solver (Skamarock et al., 2005). NEMO and WRF are coupled through the OASIS3-MCT coupler (Craig et al., 2017).

2.3. Coupled Model Configuration and Experiments

The oceanic (atmospheric) component uses an Arakawa-C grid, based on a Mercator projection at 1/12° (1/4°) resolution. The geographical domain of this coupled model is a tropical channel extending from 45°S to 45°N, with the oceanic grid being a prefect subdivision by three of the atmospheric grids. The ocean vertical grid has 75 levels, with 25 levels above 100 m and a resolution ranging from 1 m at the surface to 200 m at the bottom. The atmospheric grid has 60 eta levels with a top of the atmosphere located at 50 hPa. The WRF default vertical resolution has been multiplied by three below 800 hPa. Thus, the first 33 levels are located below 500 hPa with the first η base level located at 10 m over the ocean.

As in Samson et al. (2017), the physical package used in WRF is the longwave rapid radiative transfer model (RRTM; Mlawer et al., 1997, the "Goddard" Short Wave (SW) radiation scheme (Chou & Suarez, 1999), the "WSM6" microphysics scheme (Hong & Lim, 2006), the Betts-Miller-Janjic (BMJ) convection scheme

Table 2
Main Ocean-Atmosphere Coupled Experiments

Experiments	Mesoscale SST feedback	Current feedback
CTRL	Yes	Yes
NOCRT	Yes	No
SMTH	No	Yes

Note. All the simulations consider the large-scale SST feedback (see section 2). SST = sea surface temperature.

(Betts & Miller, 1986; Janjić, 1994), the Yonsei University (YSU) planetary boundary layer scheme (Hong et al., 2006), the unified NOAH Land Surface Model (LSM) with the surface layer scheme from MM5 (Chen & Dudhia, 2001)). WRF lateral boundary conditions are prescribed from the European Centre for Medium-Range Weather Forecasts ERA-Interim 0.75° resolution reanalysis (Dee et al., 2011) at 6-hourly intervals.

The ocean physics used in NEMO corresponds to the upstream-biased third-order scheme (UBS; Farrow & Stevens, 1995; Shchepetkin & McWilliams, 2009; Webb et al., 1998) advection for the tracers and the dynamics with no explicit diffusivity and viscosity. The vertical eddy viscosity and diffusivity coefficients are computed from a TKE turbulent closure model (Blanke & Delecluse, 1993). The oceanic open boundary conditions are prescribed with an interannual global $\frac{1}{4}°$ simulation (DRAKKAR; Brodeau et al., 2010). In order to benefit, at a limited cost, from a fully spun-up mesoscale circulation in the initial conditions of the $\frac{1}{12}°$ ocean, we first run a 5-year-long ocean forced simulation initialized from $\frac{1}{4}°$ DRAKKAR simulation and using the exact same NEMO $\frac{1}{12}°$ configuration than in our coupled simulations.

As described in Table 2, three 5-year coupled simulations are performed over the 1989–1993 period. The simulations only differ by the degree of coupling they consider. In the control run (CTRL), WRF gives NEMO hourly averages of freshwater, heat, and momentum fluxes; whereas, the ocean model sends WRF the hourly SST and surface currents. In CTRL, the surface stress is estimated using the wind relative to the ocean motions: $U_r = U_a - U_o$. Note that the use of relative winds also involves a modification of both the surface layer vertical mixing parameterization (YSU in our case) and the tridiagonal matrix for vertical turbulent diffusion (Lemarié, 2015). In NOCRT, the ocean model sends WRF only the SST. Finally, in the third simulation, hereafter called SMTH, NEMO sends WRF the surface currents and a smoothed SST. The smoothed SST fields are obtained using the filter described hereafter.

Finally, to confirm the results obtained with SMTH (see section 4 on the TFB coupling coefficients) and to test the robustness of the spatial filter, an additional coupled simulation called *SMTH_NOCRT* has been carried out. The ocean model sends WRF only the smoothed SST (the CFB is ignored). The comparison between SMTH and *SMTH_NOCRT* shows that some of the mesoscale stress (and wind) signal in SMTH is still due to the TFB as it cannot be attributed to the CFB (see section 4). To remove all the mesoscale signal, a much larger filter should be used. However, such a filter would suffer from the drawback that it could also modify the large-scale signal, which would complicate the comparison of the simulations.

2.4. Spatial Filter

Following Putrasahan et al. (2013) and Seo et al. (2015), and as described in Renault, McWilliams, Masson, et al. (2017), the mesoscale anomalies are isolated from the large-scale signal by using a spatial filter. A field ϕ is smoothed using a Gaussian spatial filter with a standard deviation of 4 (12) grid points at 1/4° (1/12°). Gaussian weights located at a distance larger than 3 standard deviation of the Gaussian (σ) are considered zero. The Gaussian filter is thus applied on a $(6\sigma + 1) \times (6\sigma + 1)$ window, which makes 25×25 points at 1/4°, or 73×73 points at 1/12°, which corresponds to≈6° × 6°. The filter cutoff is about 250 km. Land points are treated as missing data and the weights of windows including land points are renormalized over the remaining oceanic points. Mesoscale anomalies of a field ϕ are then defined as $\phi' = \phi - [\phi]$, with $[\phi]$ the smoothed field. Note that because the same filter is used in both SMTH and in the estimation of the coupling coefficients described hereafter, a larger filter cutoff would lead to similar results than the ones presented in this study.

2.5. The 10-m Wind, Equivalent Neutral Wind, and Wind Relative to the Oceanic Motions

Three different sorts of wind are defined:

- The 10-m wind U_a is defined as the wind at the first vertical level of the atmospheric model, which has been defined at ≈10 m.
- The relative wind $U_r = U_a - U_o$, with U_o being the oceanic surface current. Because the first vertical level is often not defined around 10 m, the 10-m wind is often diagnosed from the friction velocity and some atmospheric parameters. However, such a definition does not allow to estimate the absolute 10-m wind but rather the relative U_r.
- Satellite scatterometers (such as QuikSCAT) provide a 10-m wind; however, it does not correspond to U_a: it is estimated from the pseudo-stress and is reported as the so-called ENW (Bentamy et al., 2013), that is, the wind that would exist if the conditions were neutrally stable (Ross et al., 1985). As further confirmed in this study, it actually represents the ENW relative to the surface current (U_{ENWr}) rather than the absolute ENW. Following, for example, Perlin et al. (2014), the U_{ENWr} can be computed as

$$U_{\mathrm{ENWr}} = \frac{u_*}{k}\left(ln\frac{10}{z_0}\right) \quad (1)$$

  where the friction velocity u_* and roughness length z_0 (in meters) are taken at each output interval, and $k = 0.4$ is the von Karman constant.

2.6. Coupling Coefficients

Table 1 provides a synthetic description of the coupling coefficients described hereafter.

2.6.1. CFB Coupling Coefficients

As in Renault, Molemaker, Mcwilliams, et al. (2016) and Renault, McWilliams, Masson, et al. (2017), s_τ is defined as the slope of the robust regression (Li, 1985) between surface stress curl and oceanic current vorticity. It is evaluated at each grid point for both the simulations and the observations. The fields are first temporally averaged using a 29-day running mean to suppress the weather-related variability (Chelton et al., 2007), and the large-scale signal is removed using the same high-pass Gaussian spatial filter used in the simulation SMTH with a 250-km cutoff (roughly corresponding to the eddy scale, as in, for example, Seo (2017), see filter description above). Note that a 15-day running mean has the same filter cutoff frequency as the Gaussian filter used in this study (see section 2.4) but does not efficiently suppress the weather-related variability because of the sidelobes of its filter transfer function.

The s_w is defined as the slope of the regression between 10-m (or ENW) wind curl and oceanic current vorticity. It is evaluated at each grid point for both the simulations and the observations. As for s_τ, the fields are first temporally averaged using a 29-day running mean and spatially high-pass filtered.

2.6.2. TFB Coupling Coefficients Based on Derivatives

Consistent with Chelton et al. (2007) and Wang and Castelao (2016) and numerous other studies, the following coupling coefficients have been estimated for the summer period of each hemisphere: 10-m (or ENW) wind curl and cross-wind SST gradient (s_{Cu}); 10-m (or ENW) wind divergence and down-wind SST gradient (s_{Du}); wind stress curl and cross-stress SST gradient (s_{Cstr}); wind stress divergence and down-stress SST gradient (s_{Dstr}). The method used here is similar to the one applied by Chelton et al. (2007) and Wang and Castelao (2016). The cross-wind (cross-stress) and down-wind (down-stress) components of the SST gradient are computed for each daily QuikSCAT Wind U_{ENWr} (surface stress) and daily SST. Note that using 3-day-averaged field does not change the results. To remove the atmospheric synoptic variability, a 29-day running window is then applied on the cross-wind and down-wind (cross-stress and down-stress) SST gradient, wind and surface stress curl, and divergence. Anomalies of each variable are finally computed using the spatial Gaussian high-pass filter (250-km cutoff, see above). Following such a method allows to reproduce, for example, the Figure 1 from Wang and Castelao (2016). The same method is applied with the model fields.

2.6.3. TFB Coupling Coefficients Based on Mesoscale Anomalies

The coupling coefficients defined by O'Neill et al. (2012) have been computed. They are based on mesoscale SST and the magnitude of wind (s_u) or surface stress (s_{str}). As in O'Neill et al. (2017), the influence of the storms have been damped out by removing large wind speed or surface stress magnitude with values greater than 2 standard deviations σ from the time mean at each grid point. This procedure allows removing potential biases in the TFB response estimate that can be induced by the storms (atmospheric forcing vs. SST feedback). It removes less than 10% of the points. The mesoscale anomalies are then estimated using the spatial filter described above.

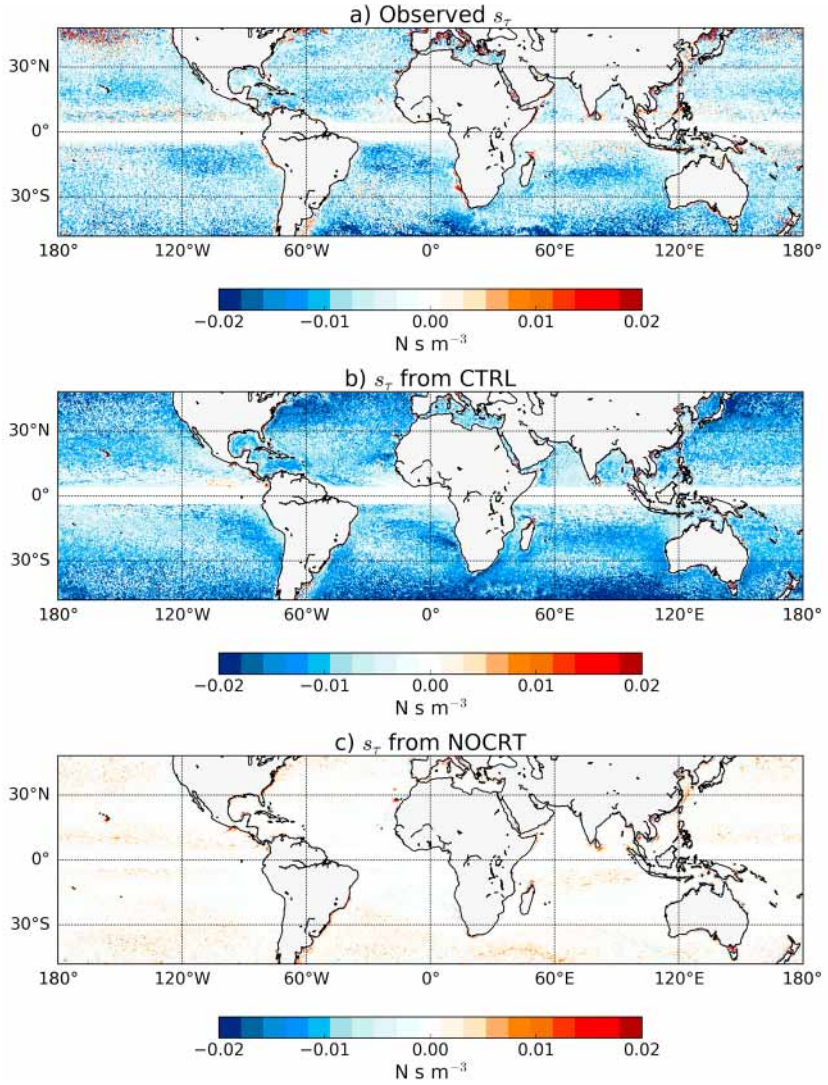

Figure 1. The current feedback to the atmosphere induces persistent surface stress anomalies that can be expressed using a linear relationship. The coupling coefficient between the surface geostrophic current vorticity and the surface stress curl (s_τ) is able to efficiently isolate the current feedback from the thermal feedback. (a) The s_τ as estimated from the observations. (b) The s_τ as estimated from CTRL. (c) The s_τ as estimated from NOCRT.

3. Disentangling the CFB

As stated in section 1, the CFB has only a systematic effect on the stress/wind curl. This is further examined in this section.

3.1. Effect on the Surface Stress Curl

The coupling coefficient between the current vorticity and the stress curl (s_τ) is estimated from satellite altimeter data (AVISO and a QuikSCAT product, as in Renault, McWilliams, Masson, et al. (2017)) and compared to CTRL and NOCRT (Figure 1). In the observations and in CTRL, s_τ is negative almost everywhere (Figures 1a and 1b): a positive surface current vorticity anomaly causes a negative surface stress curl anomaly. The s_τ can be interpreted as a measure of the CFB efficiency: the more negative a s_τ, the more efficient an eddy killing. It primarily depends on the large-scale wind: the larger the wind speed, the more negative s_τ (Renault, McWilliams, Masson, et al., 2017, and equation 17 from ; Gaube et al., 2015). The s_τ therefore partially determines the sink of energy induced by the CFB (Renault, Molemaker, Gula, et al., 2016; Xu & Scott, 2008; Xu et al., 2016), as a large sink of energy needs the presence of both an important mesoscale activity and a negative s_τ (Renault, McWilliams, Masson, et al., 2017). The s_τ in CTRL is overestimated by ≈50% with respect to the observations. While part of that discrepancy is certainly due to model

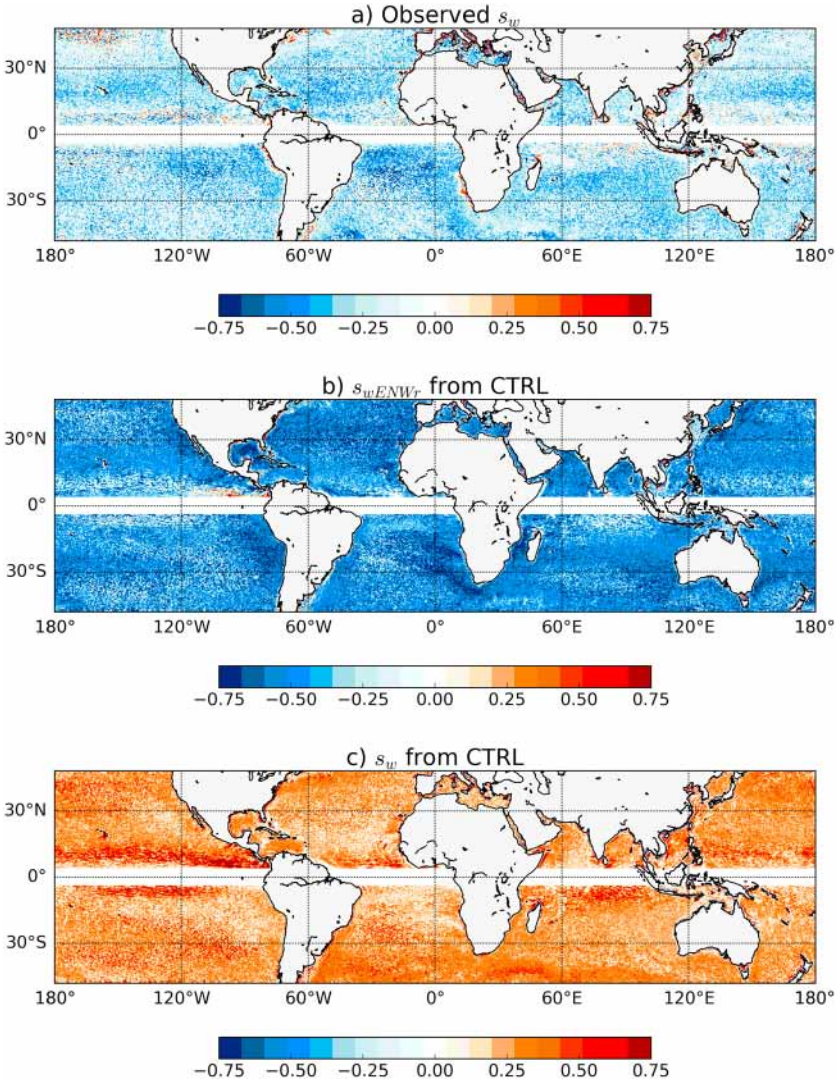

Figure 2. The current feedback to the atmosphere induces persistent surface 10-m wind anomalies that can also be expressed using a linear relationship. As s_τ, the coupling coefficient between the surface geostrophic current vorticity and the 10-m wind curl (s_w) is able to efficiently isolate the current feedback from the thermal feedback. Scatterometers such as QuikSCAT are not able to characterize the wind response to the current feedback. (a) The s_w as estimated from the observations. (b) The s_w as estimated from CTRL using the relative equivalent neutral wind wind. (c) The s_w as estimated from CTRL using the 10-m wind.

biases, there are important sampling differences between AVISO and QuikSCAT that can have a large influence on the s_τ estimate (see Figure 2 of the supporting information of Renault, McWilliams, Masson, et al., 2017). In NOCRT, where only the TFB is still active, s_τ strongly reduces (by more than 96%), becoming very weak everywhere (Figure 1c), indicating that the mesoscale surface current vorticity is not correlated with the mesoscale surface stress curl. Thus, at the mesoscale, s_τ efficiently unravels the CFB effect on the surface stress from that due to the TFB. This result is further confirmed by estimating s_τ from SMTH where the CFB is active and the mesoscale SST is ignored by the atmosphere. In such an experiment, s_τ is very similar to that estimated from CTRL (not shown).

3.2. Effect on the 10-m Wind Curl and Scatterometers Limitations

To characterize globally the wind curl response to the CFB, the coupling coefficient between the surface current vorticity and the wind curl (s_w) is first computed from CTRL using U_a. The s_τ and s_w have opposite sign (Figures 1b and 2c); that is, a positive surface current vorticity anomaly induces a negative surface stress curl anomaly, which in turn causes a positive wind curl anomaly (Renault, Molemaker, Mcwilliams, et al., 2016). The s_w varies from 0 to 0.5 with a mean value of ≈0.3. For example, it means that a mesoscale eddy with

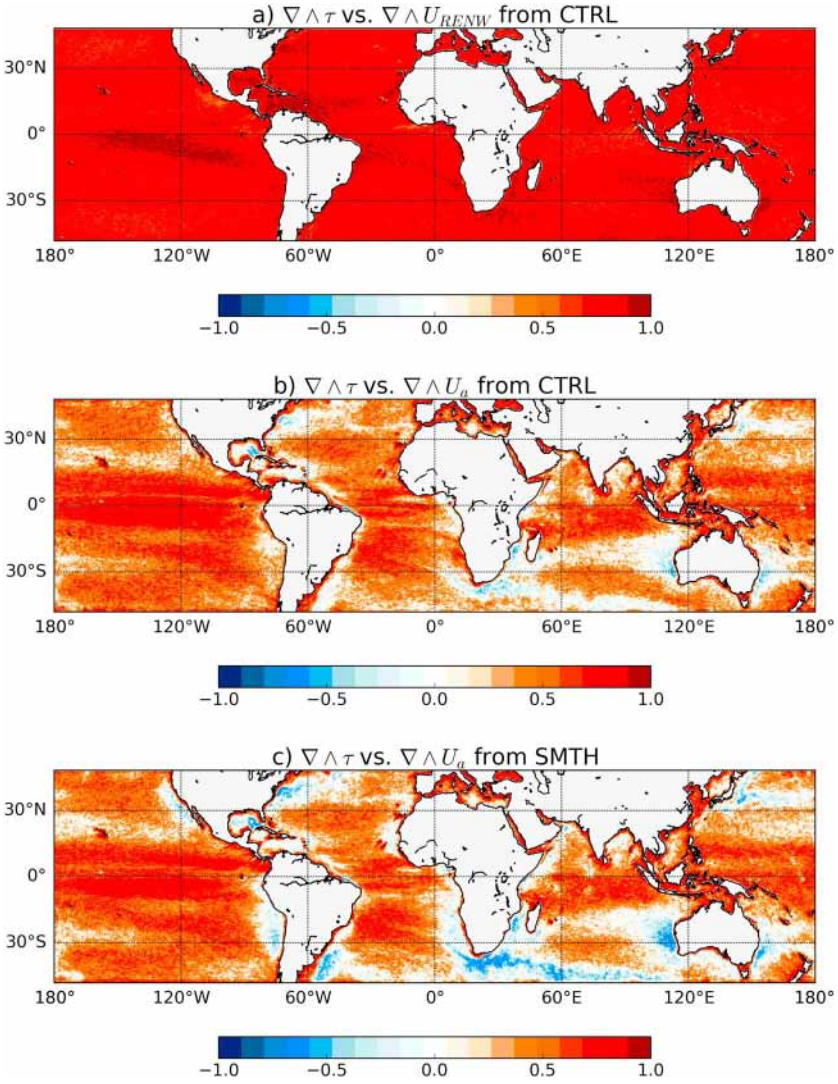

Figure 3. The surface current vorticity can partially drive the mesoscale wind curl variability. Scatterometers wind can not monitor it. a) Temporal correlations between the surface stress and the relative ENW from CTRL. b) Temporal correlations between the surface stress and the 10-m absolute wind from CTRL. c) Temporal correlations between the surface stress and the 10-m absolute wind from SMTH. The larger correlations (in red) indicate regions where the mesoscale wind determines the stress ("top-down" effect). Negative correlations highlight regions where the current forces the mesoscale wind ("bottom-up" effect).

a velocity of 1 m/s will induce on average a wind velocity anomaly of 0.3 m/s. From the atmospheric point of view, the wind response to the CFB remains weak. However, s_w can be interpreted as a measure of the efficiency of the partial reenergization of the ocean by the wind response to the CFB (Renault, Molemaker, Mcwilliams, et al., 2016): the larger s_w, the larger the partial reenergization of the mesoscale currents. For the California upwelling System, $s_w = 0.23$ and the partial reenergization is ≈25%. In NOCRT, consistent with the previous result on s_τ, s_w becomes very weak (not shown) and thus appears to be a good metric to characterize the wind response to the CFB.

Figure 2b shows that s_w evaluated from the observations and from CTRL are of opposite sign, observed s_w from satellite being negative everywhere with a mean value of ≈ -0.54. This is because QuikSCAT scatterometer winds represent U_{ENWr} (e.g., Chelton et al., 2001; Cornillon & Park, 2001; Kelly et al., 2001; Chelton et al., 2004) rather than U_{ENW} or U_a. The s_w is therefore strongly positively correlated to s_τ ($r > 0.8$). To confirm it, s_w is estimated from CTRL mimicking scatterometer winds by using the relative ENW (s_{wENWr}, Figure 2b), and by using U_r (s_{wr}). The s_{wENWr} and s_{wr} are very alike (not shown) and are a mirror of s_τ. This confirms that scatterometers can characterize the relative wind (U_r) response to the CFB; however, it would

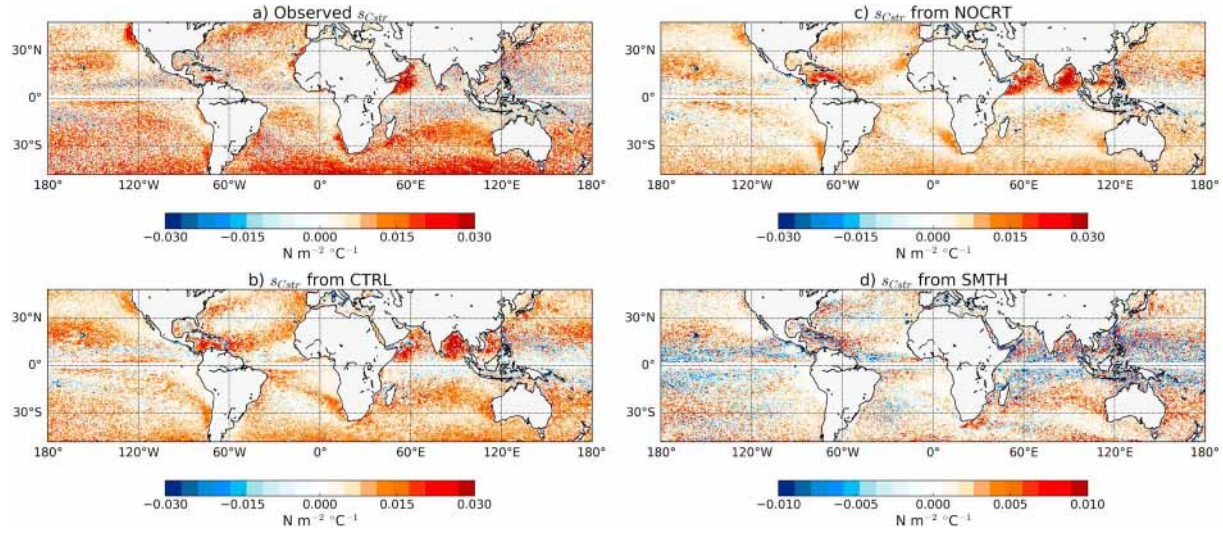

Figure 4. The coupling coefficient between the surface stress curl and the cross-wind SST (s_{Cstr}) does not properly isolate the thermal feedback from the current feedback: the current feedback can cause surface stress mesoscale features that are correlated with the cross-wind SST. Similar results are found for s_{Cu}. (a) s_{Cstr} as estimated from the observations for the summer period. (b) s_{Cstr} as estimated from CTRL for the summer period. (c) The s_{Cstr} as estimated from NOCRT for the summer period. (d) the s_{Cstr} as estimated from SMTH for the summer period (note the different color scale). Similar results are found when considering all the seasons.

be overestimated (i.e., more negative) by ≈10% because of the use of U_{ENWr} instead of U_r (not shown). Difference between U_a and U_{ENW} can be large for atmospheric stratifications that deviate greatly from neutral conditions (Song et al., 2009). This is consistent with Song et al. (2009) and Perlin et al. (2014) that show that the wind curl response to the TFB can be overestimated by ≈10% when using the ENW instead of the 10-m wind.

The limitations of scatterometry to capture the "bottom-up" effect of the CFB is further confirmed by computing the correlation between the surface stress curl and the low-level wind curl at mesoscale. Consistent with equation 1, Figure 3a shows that, at the mesoscale, scatterometer-like U_{ENWr} curl is positively correlated everywhere to the surface stress curl (similar results are found using QuikSCAT). This is logical as the wind is determined from the surface stress. On the other hand, Figure 3b shows much weaker values for the correlation between U_a and the stress curl, with even null or negative values over the western and eastern boundary currents areas. The positive correlations indicate regions where the mesoscale stress and wind curl are mainly driven by the atmospheric internal variability or by the TFB while these negative correlations highlight regions where, at the mesoscale, the currents force the lower atmosphere and dominate the TFB and the atmospheric internal variability. To confirm it, Figure 3c shows the same correlations but using the SMTH simulation (in which the SST mesoscale signal is not sent to the atmosphere). In regions characterized by a weak mesoscale activity, the atmosphere rather than the TFB determines the sign of the mesoscale wind and stress curl. Regions characterized by a large mesoscale activity (as WBCs or eastern boundary currents) have correlations between stress curl and wind curl even more negative as the TFB is removed. Those features cannot be monitored by scatterometers. Therefore, this confirms that when using scatterometers, the stress seems more appropriate to assess the atmospheric response to the air-sea interactions.

4. Disentangling the TFB

4.1. Effects on the Mesoscale Stress and Wind Curl

The coupling coefficient between the surface stress curl and the cross-stress SST gradient (s_{Cstr}, Chelton et al., 2004) is estimated from the observations and CTRL for the summer period of each hemisphere (Figures 4a and 4b, as in Chelton et al. (2007);Wang and Castelao (2016), see Methods). Consistent with, for example, Chelton et al. (2007) and Wang and Castelao (2016), in the observations, s_{Cstr} has overall values varying from 0 to 0.03 $\mathrm{N{\cdot}m^{-2}{\cdot}^{\circ}C^{-1}}$ and is larger where the wind is more intense (O'Neill et al., 2012). Offshore, in regions of weak EKE, s_{Cstr} is close to zero or not significant. In regions of intense atmospheric convection (e.g., Intertropical Convergence Zones), the atmospheric mesoscale is characterized by vortices generated by the synoptic convergent circulation and wind gusts, which force the ocean even at the mesoscale, resulting

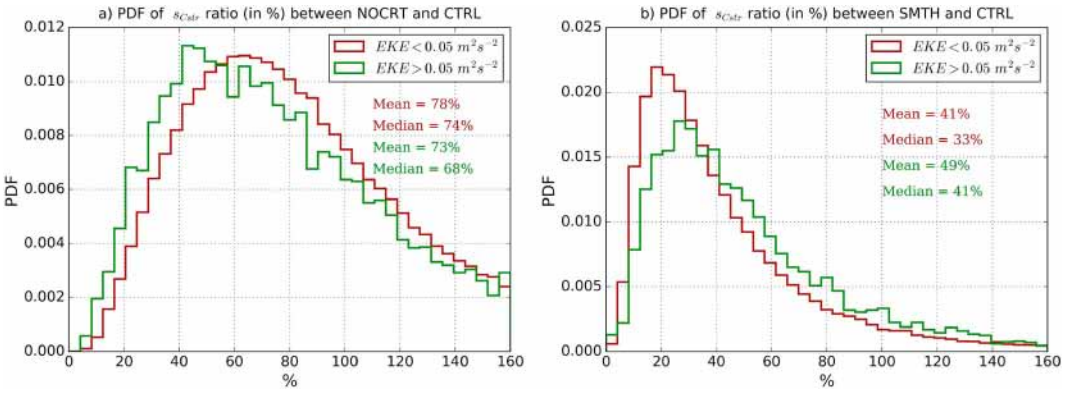

Figure 5. The current feedback can cause surface stress mesoscale features that are correlated with the cross-wind SST, contaminating the coupling coefficient s_{Cstr}. (a) Probability density function (PDF) of the ratio between s_{Cstr} as estimated from NOCRT and s_{Cstr} as estimated from CTRL. Low-level and high-level EKE regions are considered. Only positive values of s_{str} are considered, as negative values do not stand for a TFB effect. The 2°S to 2°N band that is masked as the summer of each hemisphere is considered. (b) Same as (a) but between SMTH and CTRL. Similar results are found for s_{Cu} and when considering all the seasons.

in negative s_{Cstr}. The spatial distribution of s_{Cstr} estimated from CTRL (Figure 4b) is in agreement with the observations, but its intensity is underestimated. While there is no doubt that some of these are due to model biases such as the ABL or the coastal wind representations (Perlin et al., 2014; Renault, Deutsch, et al., 2016), the estimation of s_{Cstr} also suffers from uncertainties due to the effective resolution and the sampling of the observations (Renault, McWilliams, Masson, et al., 2017). For instance, despite a larger s_{Cstr}, the correlations between stress curl and cross-stress SST gradient are weaker in the observations than in the simulations.

Scatterometers integrate not only the TFB effect on the stress but also the CFB effect. Thus, s_{Cstr} may not properly distinguish the TFB effect on the stress (and wind) from that due to the CFB. the s_{Cstr} is estimated from NOCRT, that is, the coupled simulation that ignores the CFB (Figure 4c). Surprisingly, from CTRL to NOCRT, the positive values of s_{Cstr} diminish by ≈30% (Figure 5a), likely indicating that the CFB has a nonnegligible influence on s_{Cstr}. This is especially the case in regions where the mesoscale currents are the strongest. The s_{Cstr} represents the stress curl mesoscale anomalies over SST cross-shore gradients and is thus largely influenced by the surface isotherms (Chelton et al., 2001). Geostrophic currents tend to follow isotherms, therefore, as pointed out by Chelton et al. (2001), their impact on the stress curl contaminates the correlation and the coupling coefficient between surface stress curl and crosswind SST gradient. The contamination of s_{Cstr} by the CFB is furthermore confirmed by estimating s_{Cstr} from SMTH (Figure 4d). In such a simulation, the absence of mesoscale TFB should be reflected by weak values of s_{Cstr}. However, s_{Cstr} has large values, in particular, over the WBCs and the Indian Ocean, reflecting the influence of the currents on s_{Cstr}. The s_{Cstr} in SMTH represents on average ≈35% of s_{Cstr} in CTRL and can be even larger over the most eddying regions such as the WBCs (Figure 5b). However, as explained in section 2, some of the mesoscale stress signal presents in SMTH could still be due to residual SST signal. To estimate which part of s_{Cstr} in SMTH is effectively due to the CFB, s_{Cstr} is estimated from *SMTH_NOCRT* (not shown). The s_{Cstr} in *SMTH_NOCRT* is weaker than s_{Cstr} estimated from SMTH; however, the residual of SST signal can account up to 25–30% of the s_{Cstr} estimated from SMTH. This means the CFB effect represents on average ≈25% of s_{Cstr} as estimated from CTRL. Overall, this confirms that the coupling coefficient s_{Cstr} cannot fully disentangle the TFB effect and the CFB effect on the surface stress. Finally, in all the simulations, the regions with negative values of s_{Cstr} remain roughly the same, confirming that the atmosphere forced the ocean even at the mesoscale in those regions.

Similar results are found for U_a (by estimating s_{Cu}, not shown). However, using U_{ENWr} in CTRL rather than U_a (i.e., mimicking scatterometer winds), s_{Cu} can be increased by up to 25% (not shown). This overestimation is due to the use of the relative wind: geostrophic currents tend to follow isotherms and can thus contaminate the wind curl response to the TFB (Chelton et al., 2001). Moreover, large differences between ENW and 10-m wind occur when atmospheric stratifications deviate greatly from neutral conditions (Song et al., 2009). The overestimation is larger than the previous estimate by Song et al. (2009) and Perlin et al. (2014) that reports for the Agulhas Return Current an overestimation of s_{Cu} by 10–15%. To sum up, coupling coefficients

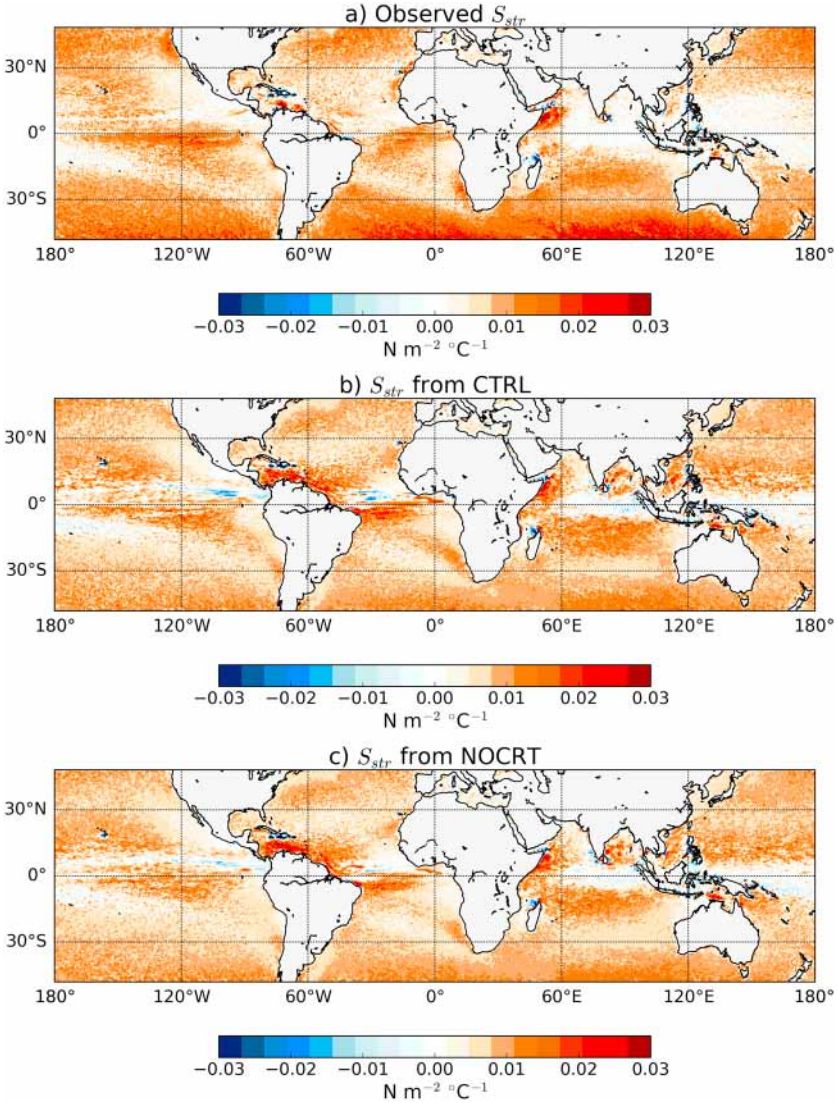

Figure 6. The coupling coefficient between the mesoscale surface stress and sea surface temperature anomalies (s_{str}) properly isolates the thermal feedback from the current feedback. Similar results are found for s_u. (a) The s_{str} as estimated from the observations. (b) The s_{str} as estimated from CTRL. (c) The s_{str} as estimated from NOCRT.

based on scatterometer observations of stress or wind curl should be used with caution when evaluating the impact of the TFB on the wind and surface stress. Finally, because the mesoscale currents are very nearly geostrophic and thus nondivergent, the CFB has little influence on the coupling coefficients s_{Du} and s_{Dstr}. As shown by Chelton et al. (2001) and numerous other studies, s_{Du} and s_{Dstr} are systematically larger (by 30% to 50%) than s_{Cu} and s_{Cstr}, which is also the case in our simulations (not shown). According to O'Neill et al. (2010), wind speed gradients contribute roughly equally to the divergence and vorticity responses to the SST. However, SST-induced crosswind and downwind gradients in wind direction enhance the divergence response to downwind SST gradients while simultaneously weakening the vorticity response to crosswind SST gradients. Chelton et al. (2001) also suggest that the effects of CFB could confuse the inference of surface currents versus SST effects on the curl of the wind or surface stress, which is true as demonstrated in this study. However, the inference of the CFB does not explain why s_{Dstr} is stronger than s_{Cstr} as the CFB increases s_{Cstr} and does not alter significantly s_{Dstr}. Therefore, the CFB can not explain why s_{Dstr} is stronger than s_{Cstr}. Finally, Schneider and Qiu (2015) suggest that these coupling coefficients could be driven by distinct physics. Stress and wind divergences result from either large-scale winds crossing the front or from a thermally direct cross-frontal circulation. The stress and wind curl responses to the TFB are expected to be larger when winds

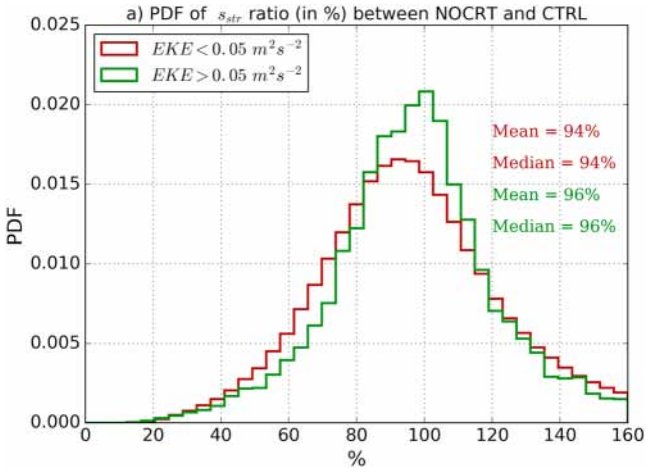

Figure 7. Probability density function of the ratio between s_{str} as estimated from NOCRT and s_{str} as estimated from CTRL. Low-level and High-level EKE regions are considered. Only positive values of s_{Cstr} are considered as negative values do not stand for a TFB effect. Confirming Figure 6, the current feedback does not influence the coupling coefficients based on stress or wind magnitude.

are parallel to SST fronts; however, they are weakened by geostrophic spindown, yielding to weaker coupling coefficients.

4.2. Mesoscale Wind and Surface Stress Magnitude

O'Neill et al. (2012) demonstrate that the mesoscale stress magnitude perturbations are characterized by a roughly linear dependence on the mesoscale SST perturbations and, to better characterize the stress magnitude response, define the surface stress coupling coefficient s_{str} (Figure 6a). Here, s_{str} is evaluated from the observations and CTRL (as in ; O'Neill et al., 2017, removing the influence of the storms, see section 2). The s_{str} generally varies from 0 to 0.03 $N{\cdot}m^{-2}{\cdot}{}^{\circ}C^{-1}$ and has larger values at the midlatitudes, in the eastern boundary currents and near some WBCs. Consistent with the previous results, s_{str} has negative values over regions of important atmospheric convection. CTRL fairly represents the s_{str} spatial distribution (Figure 6b) although it underestimates its strength in particular over the Antarctic Circumpolar Current likely because of the choice of ABL parameterization in our model simulations. ABL parameterizations behavior can strongly vary from a region to another. A dedicated sensitivity study should be considered for such a region. In NOCRT, s_{str} has a very alike spatial distribution and intensity, suggesting that the CFB does not have a significant influence on mesoscale surface stress and thus on s_{str} (Figure 6c). This is furthermore corroborated by the probability density function of the ratio between s_{str} as estimated from NOCRT and CTRL (Figure 7), that shows difference between both experiments of ≈6%. In SMTH, s_{str} is very weak, confirming the CFB does not influence its intensity. Although geostrophic currents tend to follow isotherms, the CFB does not have a systematic statistic effect on the stress magnitude as a current anomaly can induce a positive or a negative stress (wind) anomaly depending on the wind direction relative to the current direction. This is further confirmed by the comparison between SMTH and *SMTH_NOCRT*. The ratio between s_{str} as estimated from SMTH and *SMTH_NOCRT* is close to 1 shown). This indicates that the remaining s_{str} signal in SMTH is not induced by the CFB but rather by residual SST signal. Similar results are found when using U_a instead of the surface stress to estimate s_u. However, the use of U_{ENWr} instead of U_a can overestimate the TFB effect on the wind by ≈25% (not shown) because U_a and U_{ENWr} can differ when the atmospheric stratification deviates greatly from neutral conditions. This is consistent with O'Neill (2012) that report an overestimation by 10–30% based on in situ data buoys observations.

5. Discussion

Both CFB and TFB exert an influence on the wind and surface stress. While the CFB has a "bottom-up" effect from the surface current to the surface stress and the wind, the TFB has a "top-down" effect from the ABL and the 10-m wind to the surface stress. The CFB mainly affects the stress and wind curl, whereas the TFB can have an influence on their curl, divergence, and magnitude. In the last decade, coupling coefficients have been defined to evaluate the importance of the mesoscale air-sea interactions on the wind and surface stress. We show that coupling coefficients based on curl of current and stress (s_τ) or wind (s_w) efficiently allow to disentangle and characterize the influence of the mesoscale CFB on surface stress curl and 10-m wind curl. The mesoscale TFB influence on stress (wind) curl is often characterized by estimating coefficients between stress (wind) curl and cross-stress (cross-wind) SST gradient (e.g., Chelton et al., 2001, 2007; O'Neill et al., 2003, 2005). However, at the mesoscale, these TFB coupling coefficients cannot properly unravel the TFB and CFB effects. Coefficients based on divergence or mesoscale anomalies of SST and stress (or wind) allow disentangling the TFB effects from those due to the CFB. Scatterometer winds have been very useful to demonstrate the ubiquity of both TFB and CFB effects on surface stress and wind. However, consistent with Chelton et al. (2001) and Plagge et al. (2012), we show that because scatterometer winds represent the ENW relative to the oceanic motions, they allow to characterize the relative ENW response to the CFB and TFB and not the absolute wind response. Despite limitations in the estimation of wind and then surface stress by scatterometers (Quilfen et al., 2001), as scatterometers are fundamentally stress-measuring instruments, coupling coefficients based on stress appear to be more appropriate to characterize both TFB and CFB effects from scatterometers data.

The approach presented in this study is mainly based on numerical models and thus suffers from limitations that can largely affect the surface stress and wind responses to the air-sea interactions. As shown by Perlin et al. (2014) and Oerder et al. (2016), of a particular concern is the choice of the ABL mixing parameterization. For the Agulhas Return Current and the Peruvian Upwelling System, the TFB coupling coefficients in numerical models present a sensitivity to such a parameterization. In the present study, we use the YSU parameterization that has been shown to underestimate the strength of the TFB coupling coefficient in the Agulhas return current region (Perlin et al., 2014). The coupling coefficient between surface current vorticity and wind curl depends on the ABL height (Renault, McWilliams, Penven, et al., 2017). Therefore, the CFB effects on surface stress and wind may also be sensitive to the choice of the atmospheric boundary layer mixing parameterization. Futures studies similar to Perlin et al. (2014) are needed for characterizing such a sensitivity. Furthermore the results presented in this study are not necessarily valid at the submesoscale, as the ocean models used in this study are mesoscale resolving but do not permit the generation of submesoscale features. At the submesoscale, for the California upwelling system, Renault et al. (2018) show that s_τ can be contaminated by the TFB but they do not examine the other coupling coefficients. Similar studies for other regions should be carried out to assess whether the different coupling coefficients can properly isolate the TFB from the CFB at the submesoscale. Finally, in this study, a 1/4° atmospheric model has been coupled to a 1/12° oceanic model. This raises the question on the atmospheric spatial resolution needed to couple or to force an ocean model. Is an equivalent atmospheric and oceanic spatial resolution deemed to be required to represent the air-sea coupling coefficients? We intend to investigate this soon.

Our results have large implications for the understanding of the mesoscale air-sea interactions, and their effects on the ocean. Although the coupled model used is this study only covers the midlatitude ocean (45°S to 45°N), the findings presented in this study should be valid for high-latitude regions. The mesoscale stress anomalies induced by both TFB and CFB cause additional Ekman pumping that can (for the CFB) induce a sink of energy from the ocean to the atmosphere and a large dampening of the mesoscale activity (e.g., Duhaut & Straub, 2006; Gaube et al., 2015; Seo et al., 2015; Renault, Molemaker, Mcwilliams, et al., 2016; Oerder et al., 2018). For both TFB and CFB, it may impact the biogeochemical production by altering the concentration of nutrients or iron in the euphotic zone. Understanding and characterizing those feedbacks is therefore crucial to represent the mean and mesoscale ocean circulation but also the ocean production, ventilation, and carbon uptake. Finally, those results also raise the question on how to force an ocean model. Consistent with Duhaut and Straub (2006) and Chelton et al. (2007), we show that using scatterometers as a forcing can be a source of various biases mainly because they represent relative ENW wind. In addition, scatterometers surface stress already incorporates the mesoscale anomalies induced by the real eddies that are not coherent with simulated eddies by an ocean model without data assimilation. Simple parameterizations based on coupling coefficients could be used to mimic the air-sea interactions. However, to do so, the coupling coefficients should allow disentangling the TFB and CFB effects on the wind (or stress). Future satellite missions (such as SKIM (Ardhuin et al., 2017) and WaCM (Bourassa et al., 2016; Rodríguez et al., 2018) would likely allow measuring the surface stress and the surface currents in a consistent way and thus would help to better understand and characterize the ENW and surface stress responses to both TFB and CFB.

Acknowledgments
We appreciate support from the National Science Foundation (OCE-1419450). This work used the GENCI-TGCC computing resources GENCI-TGCC (grant 2017-0106895 2018-0106895 A0050107298) and the Engineering Discovery Environment (XSEDE). This work benefited from developments done during the PULSATION ANR-11-MONU-0010 project of the French National Research Agency (ANR). V. Oerder was funded by FONDECYT postdoctoral project 3180472. The authors thank Dudley Chelton, Larry O'Neill, Bertrand Chapron, and Abderrahim Bentamy for useful discussions. The authors want to thank two anonymous reviewers and Dudley Chelton for their comments. Data can be downloaded from this website (https://tinyurl.com/ycb7ob6k).

References

Anderson, L. A., McGillicuddy, D. J. Jr., Maltrud, M. E., Lima, I. D., & Doney, S. C. (2011). Impact of eddy–wind interaction on eddy demographics and phytoplankton community structure in a model of the North Atlantic Ocean. *Dynamics of Atmospheres and Oceans*, *52*(1-2), 80–94.

Ardhuin, F., Aksenov, Y., Benetazzo, A., Bertino, L., Brandt, P., Caubet, E., et al. (2017). Measuring currents, ice drift, and waves from space: The Sea Surface KInematics Multiscale monitoring (SKIM) concept. *Ocean Science*, *14*, 337–354. https://doi.org/10.5194/os-2017-65

Bentamy, A., Grodsky, S. A., Chapron, B., & Carton, J. A. (2013). Compatibility of C-and Ku-band scatterometer winds: ERS-2 and QuikSCAT. *Journal of Marine Systems*, *117*, 72–80.

Betts, A., & Miller, M. (1986). A new convective adjustment scheme. Part II: Single column tests using GATE wave, BOMEX, ATEX and Arctic air-mass data sets. *Quarterly Journal of the Royal Meteorological Society*, *112*(473), 693–709.

Blanke, B., & Delecluse, P. (1993). Variability of the tropical Atlantic Ocean simulated by a general circulation model with two different mixed-layer physics. *Journal of Physical Oceanography*, *23*(7), 1363–1388.

Bourassa, M. A., Rodriguez, E., & Chelton, D. (2016). Winds and currents mission: Ability to observe mesoscale AIR/SEA coupling. In *Geoscience and Remote Sensing Symposium (IGARSS), 2016 IEEE International* (pp. 7392–7395). IEEE.

Brodeau, L., Barnier, B., Treguier, A.-M., Penduff, T., & Gulev, S. (2010). An ERA40-based atmospheric forcing for global ocean circulation models. *Ocean Modelling*, *31*(3-4), 88–104.

Bye, J. A. (1985). Large-scale momentum exchange in the coupled atmosphere-ocean. *Elsevier Oceanography Series*, *40*, 51–61.

Chelton, D. B., Esbensen, S. K., Schlax, M. G., Thum, N., Freilich, M. H., Wentz, F. J., et al. (2001). Observations of coupling between surface wind stress and sea surface temperature in the eastern tropical Pacific. *Journal of Climate*, *14*(7), 1479–1498.
Chelton, D. B., Schlax, M. G., Freilich, M. H., & Milliff, R. F. (2004). Satellite measurements reveal persistent small-scale features in ocean winds. *Science*, *303*(5660), 978–983.
Chelton, D. B., Schlax, M. G., & Samelson, R. M. (2007). Summertime coupling between sea surface temperature and wind stress in the California Current System. *Journal of Physical Oceanography*, *37*(3), 495–517.
Chelton, D. B., Schlax, M. G., & Samelson, R. M. (2011). Global observations of nonlinear mesoscale eddies. *Progress in Oceanography*, *91*(2), 167–216.
Chelton, D. B., & Xie, S.-P. (2010). Coupled ocean-atmosphere interaction at oceanic mesoscales. *Oceanography*, *23*(4), 52–69.
Chen, F., & Dudhia, J. (2001). Coupling an advanced land surface–hydrology model with the Penn State–NCAR MM5 modeling system. Part I: Model implementation and sensitivity. *Monthly Weather Review*, *129*(4), 569–585.
Chou, M.-D., & Suarez, M. J. (1999). A solar radiation parameterization (CLIRAD-SW) for atmospheric studies. *NASA Technical Memorandum*, *10460*, 48.
Cornillon, P., & Park, K. (2001). Warm core ring velocities inferred from NSCAT. *Geophysical Research Letters*, *28*(4), 575–578.
Craig, A., Valcke, S., & Coquart, L. (2017). Development and performance of a new version of the OASIS coupler, OASIS3-MCT_3. 0. *Geoscientific Model Development*, *10*(9), 3297–3308.
Dee, D., Uppala, S., Simmons, A., Berrisford, P., Poli, P., Kobayashi, S., et al. (2011). The ERA-Interim reanalysis: Configuration and performance of the data assimilation system. *Quarterly Journal of the Royal Meteorological Society*, *137*(656), 553–597.
Desbiolles, F., Blanke, B., Bentamy, A., & Roy, C. (2016). Response of the Southern Benguela upwelling system to fine-scale modifications of the coastal wind. *Journal of Marine Systems*, *156*, 46–55.
Dewar, W. K., & Flierl, G. R. (1987). Some effects of the wind on rings. *Journal of Physical Oceanography*, *17*(10), 1653–1667.
Ducet, N., Le Traon, P.-Y., & Reverdin, G. (2000). Global high-resolution mapping of ocean circulation from TOPEX/Poseidon and ERS-1 and-2. *Journal of Geophysical Research*, *105*(C8), 19,477–19,498.
Duhaut, T. H., & Straub, D. N. (2006). Wind stress dependence on ocean surface velocity: Implications for mechanical energy input to ocean circulation. *Journal of Physical Oceanography*, *36*(2), 202–211.
Eden, C., & Dietze, H. (2009). Effects of mesoscale eddy/wind interactions on biological new production and eddy kinetic energy. *Journal of Geophysical Research*, *114*, C05023. https://doi.org/10.1029/2008JC005129
Farrow, D. E., & Stevens, D. P. (1995). A new tracer advection scheme for Bryan and Cox type ocean general circulation models. *Journal of Physical Oceanography*, *25*(7), 1731–1741.
Gaube, P., Chelton, D. B., Samelson, R. M., Schlax, M. G., & O'Neill, L. W. (2015). Satellite observations of mesoscale eddy-induced Ekman pumping. *Journal of Physical Oceanography*, *45*(1), 104–132.
Hogg, A. M. C., Dewar, W. K., Berloff, P., Kravtsov, S., & Hutchinson, D. K. (2009). The effects of mesoscale ocean–atmosphere coupling on the large-scale ocean circulation. *Journal of Climate*, *22*(15), 4066–4082.
Hong, S.-Y., & Lim, J.-O. J. (2006). The WRF single-moment 6-class microphysics scheme (WSM6). *Journal of the Korean Meteorological Society*, *42*(2), 129–151.
Hong, S.-Y., Noh, Y., & Dudhia, J. (2006). A new vertical diffusion package with an explicit treatment of entrainment processes. *Monthly Weather Review*, *134*(9), 2318–2341.
Hutchinson, D. K., Hogg, A. M. C., & Blundell, J. R. (2010). Southern Ocean response to relative velocity wind stress forcing. *Journal of Physical Oceanography*, *40*(2), 326–339.
Janjić, Z. I. (1994). The step-mountain ETA coordinate model: Further developments of the convection, viscous sublayer, and turbulence closure schemes. *Monthly Weather Review*, *122*(5), 927–945.
Kelly, K. A., Dickinson, S., McPhaden, M. J., & Johnson, G. C. (2001). Ocean currents evident in satellite wind data. *Geophysical Research Letters*, *28*(12), 2469–2472.
Lemarié, F. (2015). Numerical modification of atmospheric models to include the feedback of oceanic currents on air-sea fluxes in ocean-atmosphere coupled models (Technical Report RT-464). INRIA: INRIA Grenoble - Rhône-Alpes ; Laboratoire Jean Kuntzmann; Universite de Grenoble I - Joseph Fourier.
Li, G. (1985). Robust regression. *Exploring Data Tables, Trends, and Shapes*, *281*, U340.
Liu, W. T., & Tang, W. (1996). Equivalent neutral wind (NASA Technical Report). Pasedena, CA: National Aeronautics and Space Administration.
Liu, W. T., Xie, X., & Niiler, P. P. (2007). Ocean–atmosphere interaction over Agulhas extension meanders. *Journal of Climate*, *20*(23), 5784–5797.
Luo, J.-J., Masson, S., Roeckner, E., Madec, G., & Yamagata, T. (2005). Reducing climatology bias in an ocean-atmosphere CGCM with improved coupling physics. *Journal of Climate*, *18*(13), 2344–2360.
Ma, X., Jing, Z., Chang, P., Liu, X., Montuoro, R., Small, R. J., et al. (2016). Western boundary currents regulated by interaction between ocean eddies and the atmosphere. *Nature*, *535*(7613), 533–537.
Madec, G., & The NEMO team (2015). NEMO ocean engine.
McClean, J. L., Bader, D. C., Bryan, F. O., Maltrud, M. E., Dennis, J. M., Mirin, A. A., et al. (2011). A prototype two-decade fully-coupled fine-resolution CCSM simulation. *Ocean Modelling*, *39*(1), 10–30.
McWilliams, J. C. (2008). The nature and consequences of oceanic eddies. *Ocean Modeling in an Eddying Regime*, *177*, 5–15.
Mlawer, E. J., Taubman, S. J., Brown, P. D., Iacono, M. J., & Clough, S. A. (1997). Radiative transfer for inhomogeneous atmospheres: RRTM, a validated correlated-k model for the longwave. *Journal of Geophysical Research*, *102*(D14), 16,663–16,682.
O'Neill, L. W. (2012). Wind speed and stability effects on coupling between surface wind stress and SST observed from buoys and satellite. *Journal of Climate*, *25*(5), 1544–1569.
O'Neill, L. W., Chelton, D. B., & Esbensen, S. K. (2003). Observations of SST-induced perturbations of the wind stress field over the Southern Ocean on seasonal timescales. *Journal of Climate*, *16*(14), 2340–2354.
O'Neill, L. W., Chelton, D. B., & Esbensen, S. K. (2010). The effects of SST-induced surface wind speed and direction gradients on midlatitude surface vorticity and divergence. *Journal of Climate*, *23*(2), 255–281.
O'Neill, L. W., Chelton, D. B., & Esbensen, S. K. (2012). Covariability of surface wind and stress responses to sea surface temperature fronts. *Journal of Climate*, *25*(17), 5916–5942.
O'Neill, L. W., Haack, T., Chelton, D. B., & Skyllingstad, E. (2017). The Gulf Stream Convergence Zone in the time-mean winds. *Journal of the Atmospheric Sciences*, *74*(7), 2383–2412.
O'neill, L. W., Chelton, D. B., Esbensen, S. K., & Wentz, F. J. (2005). High-resolution satellite measurements of the atmospheric boundary layer response to SST variations along the Agulhas Return Current. *Journal of Climate*, *18*(14), 2706–2723.

Oerder, V., Colas, F., Echevin, V., Masson, S., Hourdin, C., Jullien, S., et al. (2016). Mesoscale SST–wind stress coupling in the Peru–Chile current system: Which mechanisms drive its seasonal variability? *Climate Dynamics*, *47*(7-8), 2309–2330.

Oerder, V., Colas, F., Echevin, V., Masson, S., & Lemarié, F. (2018). Impacts of the mesoscale ocean-atmosphere coupling on the Peru-Chile ocean dynamics: The current-induced wind stress modulation. *Journal of Geophysical Research: Oceans*, *123*, 812–833. https://doi.org/10.1002/2017JC013294

Pacanowski, R. (1987). Effect of equatorial currents on surface stress. *Journal of Physical Oceanography*, *17*(6), 833–838.

Perlin, N., De Szoeke, S. P., Chelton, D. B., Samelson, R. M., Skyllingstad, E. D., & O'Neill, L. W. (2014). Modeling the atmospheric boundary layer wind response to mesoscale sea surface temperature perturbations. *Monthly Weather Review*, *142*(11), 4284–4307.

Plagge, A. M., Vandemark, D., & Chapron, B. (2012). Examining the impact of surface currents on satellite scatterometer and altimeter ocean winds. *Journal of Atmospheric and Oceanic Technology*, *29*(12), 1776–1793.

Putrasahan, D. A., Miller, A. J., & Seo, H. (2013). Isolating mesoscale coupled ocean–atmosphere interactions in the Kuroshio Extension region. *Dynamics of Atmospheres and Oceans*, *63*, 60–78.

Quilfen, Y., Chapron, B., & Vandemark, D. (2001). The ERS scatterometer wind measurement accuracy: Evidence of seasonal and regional biases. *Journal of Atmospheric and Oceanic Technology*, *18*(10), 1684–1697.

Renault, L., Deutsch, C., McWilliams, J. C., Frenzel, H., Liang, J.-H., & Colas, F. (2016). Partial decoupling of primary productivity from upwelling in the California current system. *Nature Geoscience*, *9*, 505–508.

Renault, L., McWilliams, J. C., & Gula, J. (2018). Dampening of submesoscale currents by air-sea stress coupling in the Californian upwelling system. *Scientific Reports*, *8*(1), 13388.

Renault, L., McWilliams, J. C., & Masson, S. (2017). Satellite observations of imprint of oceanic current on wind stress by air-sea coupling. *Scientific Reports*, *7*(1), 17747.

Renault, L., McWilliams, J. C., & Penven, P. (2017). Modulation of the Agulhas Current retroflection and leakage by oceanic current interaction with the atmosphere in coupled simulations. *Journal of Physical Oceanography*, *47*(8), 2077–2100.

Renault, L., Molemaker, M. J., Gula, J., Masson, S., & McWilliams, J. C. (2016). Control and stabilization of the Gulf Stream by oceanic current interaction with the atmosphere. *Journal of Physical Oceanography*, *46*(11), 3439–3453.

Renault, L., Molemaker, M. J., Mcwilliams, J. C., Shchepetkin, A. F., Lemarié, F., Chelton, D., et al. (2016). Modulation of wind work by oceanic current interaction with the atmosphere. *Journal of Physical Oceanography*, *46*(6), 1685–1704.

Renault, L., Marchesiello, P., Masson, S., & McWilliams, J. C. (2019). Remarkable control of western boundary currents by Eddy Killing, a mechanical air-sea coupling process. *Geophysical Research Letters*, *46*. https://doi.org/10.1029/2018GL081211

Reynolds, R. W., Smith, T. M., Liu, C., Chelton, D. B., Casey, K. S., & Schlax, M. G. (2007). Daily high-resolution-blended analyses for sea surface temperature. *Journal of Climate*, *20*(22), 5473–5496.

Rio, M.-H., Mulet, S., & Picot, N. (2014). Beyond GOCE for the ocean circulation estimate: Synergetic use of altimetry, gravimetry, and in situ data provides new insight into geostrophic and Ekman currents. *Geophysical Research Letters*, *41*, 8918–8925. https://doi.org/10.1002/2014GL061773

Rodríguez, E., Wineteer, A., Perkovic-Martin, D., Gál, T., Stiles, B. W., Niamsuwan, N., & Monje, R. R. (2018). Estimating ocean vector winds and currents using a Ka-band pencil-beam Doppler scatterometer. *Remote Sensing*, *10*(4), 576.

Rooth, C., & Xie, L. (1992). Air-sea boundary layer dynamics in the presence of mesoscale surface currents. *Journal of Geophysical Research*, *97*(C9), 14,431–14,438.

Ross, D. B., Overland, J., Plerson, W. J., Cardone, V. J., McPherson, R. D., & Yu, T.-W. (1985). Oceanic surface winds. *Advances in Geophysics*, *27*, 101–140.

Samson, G., Masson, S., Durand, F., Terray, P., Berthet, S., & Jullien, S. (2017). Roles of land surface albedo and horizontal resolution on the Indian summer monsoon biases in a coupled ocean–atmosphere tropical-channel model. *Climate Dynamics*, *48*(5-6), 1571–1594.

Schneider, N., & Qiu, B. (2015). The atmospheric response to weak sea surface temperature fronts. *Journal of the Atmospheric Sciences*, *72*(9), 3356–3377.

Seo, H. (2017). Distinct influence of air–sea interactions mediated by mesoscale sea surface temperature and surface current in the Arabian Sea. *Journal of Climate*, *30*(20), 8061–8080.

Seo, H., Miller, A. J., & Norris, J. R. (2015). Eddy-wind interaction in the California Current System: Dynamics and impacts. *Journal of Physical Oceanography*, *46*(2015), 439–459.

Shchepetkin, A. F., & McWilliams, J. C. (2009). Correction and commentary for "Ocean forecasting in terrain-following coordinates: Formulation and skill assessment of the regional ocean modeling system" by Haidvogel et al. *Journal of Computational Physics*, *228*(24), 8985–9000.

Skamarock, W. C., Klemp, J. B., Dudhia, J., Gill, D. O., Barker, D. M., Wang, W., & Powers, J. G. (2005). A Description of the Advanced Research WRF Version 2. NCAR Technical Note NCAR/TN-468+STR, Mesoscale and Microscale Meteorolgy Division. Boulder, CO: National Center for Atmospheric Research. https://doi.org/10.5065/D6DZ069T

Small, R., deSzoeke, S. P., Xie, S., O'Neill, L., Seo, H., Song, Q., et al. (2008). Air–sea interaction over ocean fronts and eddies. *Dynamics of Atmospheres and Oceans*, *45*, 274–319.

Small, R. J., Richards, K. J., Xie, S.-P., Dutrieux, P., & Miyama, T. (2009). Damping of tropical instability waves caused by the action of surface currents on stress. *Journal of Geophysical Research*, *114*, C04009. https://doi.org/10.1029/2008JC005147

Song, Q., Chelton, D. B., Esbensen, S. K., Thum, N., & O'Neill, L. W. (2009). Coupling between sea surface temperature and low-level winds in mesoscale numerical models. *Journal of Climate*, *22*(1), 146–164.

Stammer, D. (1997). Global characteristics of ocean variability estimated from regional TOPEX/POSEIDON altimeter measurements. *Journal of Physical Oceanography*, *27*(8), 1743–1769.

Takatama, K., & Schneider, N. (2017). The role of back pressure in the atmospheric response to surface stress induced by the Kuroshio. *Journal of the Atmospheric Sciences*, *74*(2), 597–615.

Wang, Y., & Castelao, R. M. (2016). Variability in the coupling between sea surface temperature and wind stress in the global coastal ocean. *Continental Shelf Research*, *125*, 88–96.

Webb, D. J., De Cuevas, B. A., & Richmond, C. S. (1998). Improved advection schemes for ocean models. *Journal of Atmospheric and Oceanic Technology*, *15*(5), 1171–1187.

Wunsch, C., & Stammer, D. (1995). The global frequency-wavenumber spectrum of oceanic variability estimated from TOPEX/POSEIDON altimetric measurements. *Journal of Geophysical Research*, *100*(C12), 24,895–24,910.

Xu, Y., & Scott, R. B. (2008). Subtleties in forcing eddy resolving ocean models with satellite wind data. *Ocean Modelling*, *20*(3), 240–251.

Xu, C., Zhai, X., & Shang, X.-D. (2016). Work done by atmospheric winds on mesoscale ocean eddies. *Geophysical Research Letters*, *43*, 12,174–12,180. https://doi.org/10.1002/2016GL071275